Enhancing Trimble Applanix POSPac IN-Fusion+ PP-RTX performance in urban canyons with a novel GNSS outlier detection method

Jau-Hsiung Wang, *Trimble Navigation Limited*

Biography

Dr. Jau-Hsiung Wang is a Principal Navigation Engineer at Trimble Applanix, specializing in GNSS/INS integration and advanced navigation algorithm and software development. He earned his Ph.D. in Geomatics Engineering from the University of Calgary, where his research on intelligent MEMS INS/GNSS integration received multiple international awards. With over two decades of experience in GNSS, sensor fusion, and precise positioning, Dr. Wang holds several patents and has published extensively in IEEE and navigation journals. His innovations have advanced mobile mapping, autonomous navigation, and high-precision GNSS technologies worldwide.

Abstract

Trimble Applanix's Positioning and Orientation System Post-Processing (POSPac) is the industry-leading software suite that uses GNSS and inertial technologies to provide direct georeferencing for mobile mapping sensors across air, land, and marine platforms. Released in 2025, Trimble ProPoint single base Real-Time Kinematics (RTK) has been integrated into POSPac to enhance georeferencing robustness in GNSS-challenging environments by leveraging modern GNSS signals and advanced filtering. When a dedicated base station is impractical, Trimble CenterPoint® Real-Time eXtended (RTX) offers a valuable alternative. However, RTX performance can degrade significantly in urban canyons where multipath, signal blockage, and interference introduce multiple measurement outliers and lead to unreliable solutions. These degraded RTX outputs often underestimate their uncertainties, destabilizing GNSS-inertial integration and causing inertial navigation jumps. Existing GNSS outlier detection approaches such as Receiver Autonomous Integrity Monitoring (RAIM), fading carrier-to-noise based checks, and methods relying on external sensors or 3D maps struggle when outliers occur simultaneously or when additional data sources are unavailable.

This paper presents a new GNSS outlier detection method designed to improve IN-Fusion+ Post-Processing RTX (PP-RTX) performance in harsh urban environments without relying on external data. The method monitors pseudorange or code biases and constructs a per-satellite bias model from benign GNSS conditions. When operating in urban canyons, multipath and interference distort the computed code biases. The deviation between measured biases and the established model is used to estimate multipath and positioning errors. These estimates enable effective detection of large-error RTX solutions and improved RTX error modeling within the GNSS-inertial fusion filter. The method has resulted in two patent applications.

The approach was evaluated using over 65-hours of downtown Toronto datasets collected with five Trimble Applanix mobile-mapping systems. Reference trajectories were generated using tightly coupled Trimble ProPoint single base RTK with a navigation grade IMU. Results show that the proposed method identifies major RTX outliers and reduces PP-RTX position error by 87.84% at 1σ and 94.39% at 2σ. Incorporating the method into IN-Fusion+ PP-RTX improves post-processed position accuracy by about 44.37% at 1σ and 57.92% at 2σ.

1. Introduction

GNSS positioning relies on the line-of-sight (LOS) satellite signals to determine ranges from known satellite positions to unknown user locations on land, at sea, in the air, and in space. In harsh environments, GNSS signals are often degraded by multipath, attenuation, and interference, resulting in multiple outliers in the measurements. These outliers are difficult to model and mitigate within standard GNSS estimation frameworks, leading to unpredictable positioning accuracy. This issue is a long-standing challenge in the GNSS industry and a major performance limitation for GNSS–inertial systems. When erroneous

GNSS solutions with underestimated variances are integrated, they are overweighted in the filter and cause jumps in inertial navigation solutions.

Numerous techniques have been introduced to address this problem. Receiver Autonomous Integrity Monitoring (RAIM) performs consistency checks across position solutions derived from subsets of visible satellites and has been widely applied in navigation (Brown, 1996) (Kuusniemi et al., 2007). However, RAIM requires high measurement redundancy and assumes no more than one fault at a time, making it ineffective in harsh environments where multipath and non-line-of-sight (NLOS) conditions introduce multiple simultaneous outliers. Castaldo and etc. (2014) apply original and modified Random Sample Consensus (RANSAC) algorithms to detect multiple satellite failures by comparing position estimates from four-satellite subsets containing pseudoranges not contributing to the solution. The drawback is that the method works only when the number of outliers is smaller than the number of satellites in view minus six. Although improvements were shown for a static GPS-only dataset, further validation on larger and kinematic GNSS datasets is still required.

Wang and Gao (2007) develop a fuzzy inference system to classify high-sensitivity GPS solutions in different environments using satellite geometry and fading carrier-to-noise (C/N_0) ratio information. This method provides some benefit but is limited because fading C/N_0 is not a direct measure of multipath error and only indicates its likelihood. Anyaegbu and Hansen (2022) present a GNSS foresight service that uses a high-resolution 3D map and precise satellite orbital predictions to identify LOS signals and provide real-time GNSS performance forecasts in urban areas. Although the ratio between identified LOS and used satellites correlates with positioning accuracy, a direct functional relationship with position error is lacking. Li et al. (2022) detects faulty GNSS solutions by comparing GNSS positions with LiDAR-observed target positions, but this approach requires additional sensors, a pre-built global point-cloud map, and increased computational complexity.

In this paper, we introduce a new GNSS outlier detection method that remains effective in the presence of multiple outliers and does not require external information beyond raw GNSS measurements. The method monitors GNSS code biases and constructs a code bias model for each satellite signal under benign GNSS conditions. When operating in harsh environments, the computed code biases are distorted by multipath and interference, producing deviations from the established model. The difference between the computed bias and the predicted model, termed the code bias deviation, is used to estimate multipath and positioning errors. These estimated errors are applied to detect outliers in Trimble RTX solutions and to enhance error modeling for GNSS-inertial data fusion, improving Trimble Applanix POSPac IN-Fusion+ PP-RTX performance in challenging urban environments.

The remainder of this paper is organized as follows: Section 2 describes Trimble CenterPoint RTX and Trimble Applanix IN-Fusion+ PP-RTX technologies. Section 3 presents the proposed Code Bias based GNSS Outlier Detection (CBGOD) algorithm. Section 4 presents field test results, and Section 5 concludes the paper.

2. Trimble CenterPoint PP-RTX and Trimble Applanix IN-Fusion+ PP-RTX technology

2.1 Trimble CenterPoint PP-RTX

Trimble CenterPoint PP-RTX is a precise positioning technology designed to deliver centimeter-level accuracy without requiring local reference stations (Leandro et al., 2011). The approach relies on a globally distributed network of GNSS monitoring stations that continuously collect multi-constellation, multi-frequency observations as shown in Figure 1. These data streams are transmitted to Trimble processing centers, where precise satellite orbit, clock, and atmospheric products are generated. When used within POSPac, these corrections enable accurate positioning using only rover measurements and a valid PP-RTX subscription, providing a fully self-contained workflow that is independent of any local infrastructure.

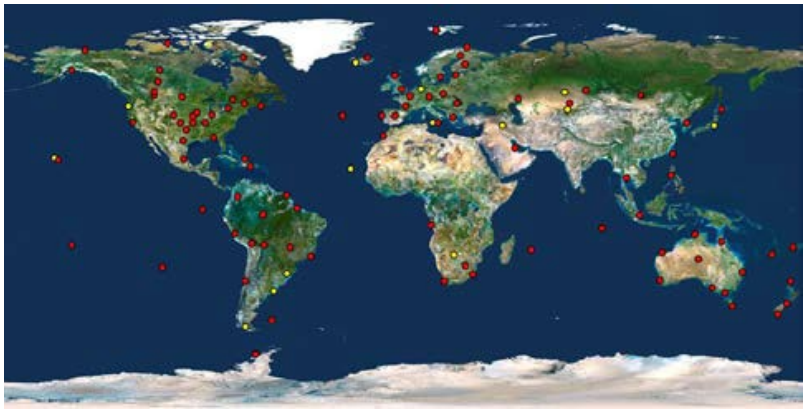

Figure 1 Trimble CenterPoint RTX tracking network

PP-RTX incorporates modern signals across GPS, GLONASS, Galileo, BeiDou-III, and QZSS, providing stronger measurement geometry and increased robustness. The correction service supports two atmospheric modeling regions: a high-density regional model over North America and Central Europe, known as the "Fast" zone, and a global model covering all remaining locations. In the Fast region, convergence typically occurs within two minutes. Outside this zone, the latest PP-RTX consistently reduces convergence time to below three minutes with Beidou-III satellites. Forward-backward smoothing removes any residual transients, yielding a continuous, high-accuracy trajectory. Once converged, PP-RTX provides stable performance with horizontal accuracy better than 3 cm and vertical accuracy better than 6 cm (Hutton et al., 2016). Achieving this level of accuracy requires appropriate GNSS antenna calibration, adequate satellite visibility, and sufficient data duration to ensure filter stabilization. Figure 2 illustrates the PP-RTX position accuracy of typical airborne data.

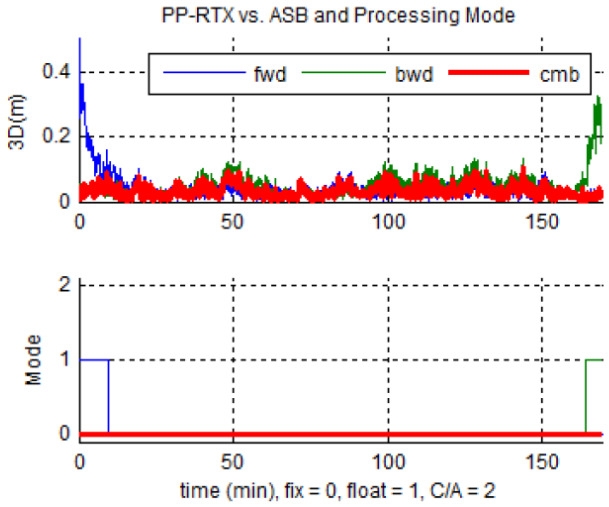

Figure 2 Forward, backward and combined PP-RTX vs. Applanix Smart Base (ASB™) and processing mode (Hutton et al., 2016)

2.2 Trimble Applanix IN-Fusion+ PP-RTX

Trimble Applanix IN-Fusion+ is an advanced aided inertial navigation system that continuously corrects INS errors using multiple aiding sensors. By optimally fusing data from GNSS and other sensors, it prevents error growth and enables high-accuracy positioning and orientation even with smaller, lower-cost IMUs. The system is built around a sophisticated Kalman filter with advanced sensor error models and supports multiple aiding sources to deliver robust, high-precision navigation for mobile mapping and positioning applications (Scherzinger, B & Hutton, J., 2020). Trimble Applanix IN-Fusion+ PP-RTX

integrates the Trimble RTX correction framework directly into POSPac's tightly coupled GNSS-inertial engine. Unlike the earlier implementation, which required users to upload trajectories to a cloud service for correction generation, the updated design automatically retrieves the necessary datasets during post-processing. For operations where internet connectivity is unavailable, Trimble hardware capable of receiving RTX via L-Band can record broadcast corrections during data collection. These corrections can then be recovered and applied within POSPac, enabling precise positioning in remote environments.

Figure 3 illustrates the architecture of IN-Fusion+ PP-RTX technology comprising an "aided-inertial" navigation system or Aided INS with aiding sensor components and Trimble CenterPoint PP-RTX. The IMU outputs incremental velocities and angles in its sensor coordinate frame. These measurements are integrated by the inertial navigator to determine the current IMU position, velocity, and orientation. A Kalman filter based error estimator ingests aiding measurements from the GNSS receivers, a Distance Measurement Indicator (DMI), and precise PP-RTX data. Using established inertial and aiding sensor error models, the filter estimates the corresponding INS and sensor errors. These estimates are fed to an error controller, which applies the necessary corrections to the inertial navigator, forming a closed-loop error control architecture that constrains inertial drift and ensures stable navigation performance.

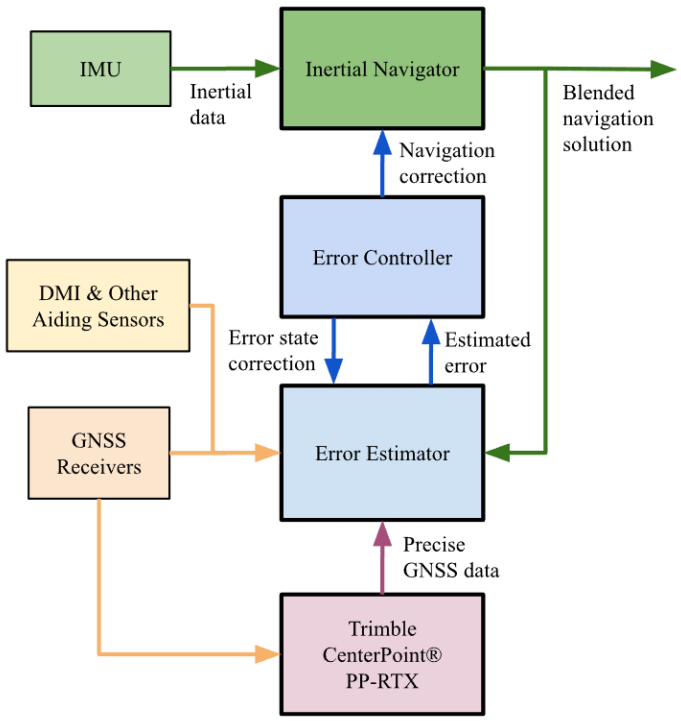

Figure 3 Trimble Applanix IN-Fusion+ PP-RTX architecture

Achieving robust filter performance depends on accurate inertial and aiding sensor error models. For land applications in GNSS challenging environments, PP-RTX measurement errors are difficult to model due to strong multipath and signal attenuation. In contrast to single base RTK where between-receiver differencing removes ionospheric and tropospheric errors the PP-RTX estimator must separate atmospheric errors from multipath using only absolute observations. Consequently, PP-RTX encounters greater challenges in detecting GNSS outliers and maintaining reliable positioning in dense urban environments.

3. Code bias based GNSS outlier detection (CBGOD) method.

This section presents a new Code Bias based GNSS Outlier Detection (CBGOD) method to detect outliers in PP-RTX solutions and to enhance GNSS error modeling in IN-Fusion+ PP-RTX.

3.1 CBGOD architecture

Figure 4 illustrates the architecture of CBGOD. GNSS observables from the receiver are first processed by the PP-RTX Estimator to compute the receiver position. These GNSS observables together with the corresponding PP-RTX positions are then provided to the Code Bias Estimator to compute the code biases for each satellite's primary signal (i.e., L1 for GPS, GLONASS, and QZSS; E1 for Galileo; and B1C for BeiDou). After a sufficient number of code bias estimates derived from precise Fixed PP-RTX solutions have been accumulated, code bias models for each satellite's primary signal are generated using the least-squares polynomial fitting method. Once the code bias models are available, the code bias estimates are further processed by the Code Multipath and Position Error Estimator to derive multipath errors and position error estimates. These estimates are then used for GNSS outlier detection and error modeling within the IN-Fusion+ PP-RTX sensor fusion framework. In post-processing, all mission data can first be used to generate the code bias models and then reprocessed to compute multipath and position error estimates for outlier detection.

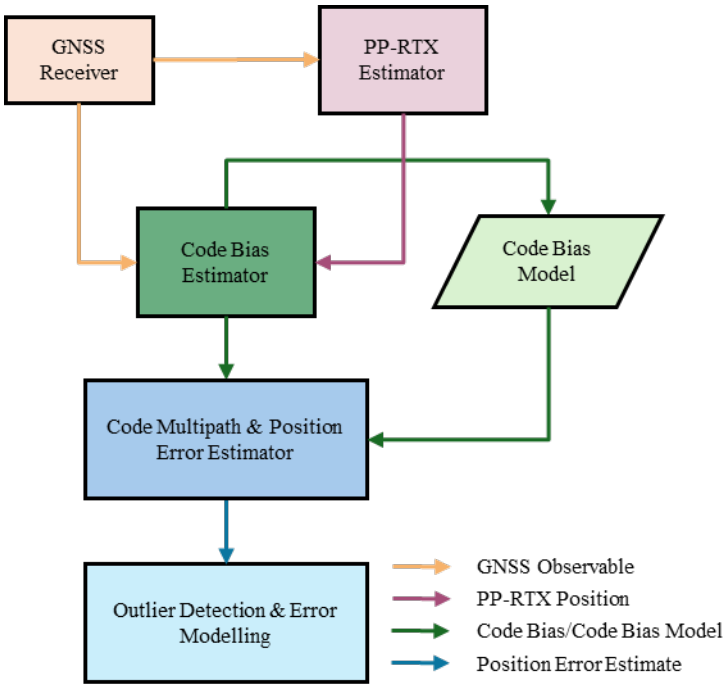

Figure 4 CBGOD architecture

3.2 Code bias estimator and code bias model

Code bias estimator processes GNSS observables and the PP-RTX positions to compute the code biases of each satellite's major signal. GNSS pseudorange or code observable from the kth satellite ρ^k can be modeled as

$$\rho^k = \hat{r}^k + c\left(d\hat{T} - d\hat{t}^k\right) + b^k + \varepsilon_\rho^k \qquad (1)$$

where $\hat{r}^k$ is the estimated user-to-satellite geometric range
$d\hat{T}$ is the estimated receiver clock offset,
$d\hat{t}^k$ is the modelled satellite clock error,
b^k is the remaining error in satellite clocks, ionosphere delay, troposphere delay, etc.,
ε_ρ^k is the code multipath and noise,

Rewrite equation (1), the remaining errors hereafter called code bias can be computed using Equation (2)

$$b^k = \rho^k - \hat{r}^k - c\left(d\hat{T} - d\hat{t}^k\right) + \varepsilon_\rho^k \quad (2)$$

The estimated user-to-satellite geometric range, $\hat{r}^k$, can be computed using Equation (3) where the receiver position $\mathbf{x} = (x, y, z)$ is provided by the PP-RTX estimator and the satellite position $\mathbf{x^k} = (x^k, y^k, z^k)$ for satellite-k is computed using GNSS ephemeris. The estimated receiver clock offset is provided by the PP-RTX estimator, and the modelled satellite clock error is computed using GNSS ephemeris.

$$r^k = \sqrt{(x^k - x)^2 + (y^k - y)^2 + (z^k - z)^2} = \left\|\mathbf{x^k} - \mathbf{x}\right\| \quad (3)$$

In benign GNSS environments, ε_ρ^k is small and is primarily dominated by random noise with a Gaussian distribution. The errors in the estimated user-to-satellite geometric range and receiver clock offset are correlated with the Fixed PP-RTX position errors, which are at the centimeter level. Under these conditions, the code bias mainly consists of meter-level errors originating from satellite clock errors, ionospheric delay, and tropospheric delay, all of which vary slowly over time. Figure 5 presents examples of the computed code bias for different satellites in open-sky conditions.

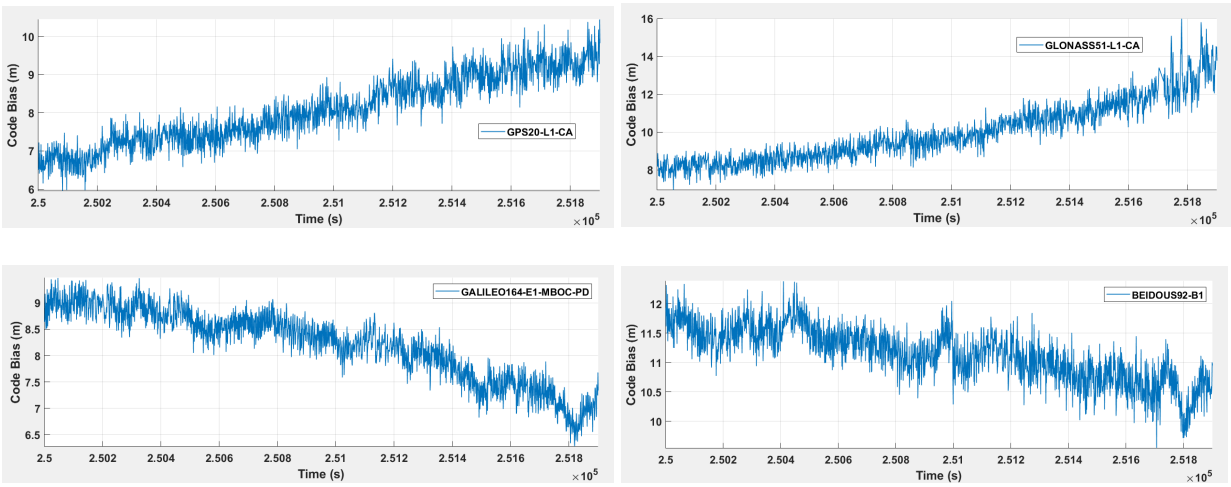

Figure 5 Code biases in GNSS benign areas

As the code bias varies slowly over time, it is modeled using a second-order polynomial, as shown in Equation (4). The least-squares polynomial fitting method (Gangi and Shapiro, 1997) is then applied to obtain the optimal fit to the data in the least-squares sense.

$$b_m^k = a_2^k t^2 + a_0^k t + a_0^k \quad (4)$$

where a_0^k, $a_1^k, and\ a_2^k$ are the code bias model coefficients for satellite k, t is GPS time and b_m^k is the expected code bias for satellite k computed by the model.

Figure 6 presents examples of the code bias models for different satellites obtained using the least-squares polynomial fitting method. The results show that the proposed model provides a good fit for the data. The residual differences between the estimated code biases and the fitted model are primarily due to random noise, with magnitudes on the order of approximately 1 m.

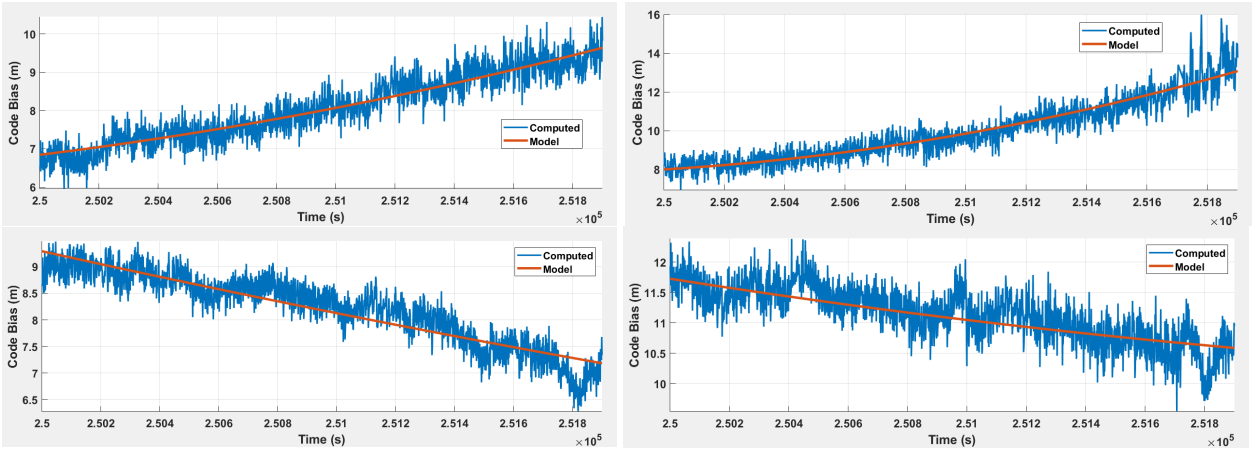

Figure 6 Code biases and code biases models

3.3 Code multipath and position error estimator

In GNSS harsh environments, the code bias is modeled as:

$$b^k = \rho^k - (\hat{r}^k + \delta\hat{r}^k) - c\left(d\hat{T} - d\hat{t}^k\right) + \varepsilon_\rho^k \tag{5}$$

where $\delta\hat{r}^k$ is the error of estimated user-to-kth satellite geometric range projected by the receiver position error. In this case the difference between the computed and expected code bias, hereafter called code bias deviation δb^k for the satellite k, can be computed as:

$$\begin{aligned}\delta b^k &= b^k - b_m^k \\ &= \rho^k - (\hat{r}^k + \delta\hat{r}^k) - c\left(d\hat{T} - d\hat{t}^k\right) + \varepsilon_\rho^k - \rho^k + \hat{r}^k + c\left(d\hat{T} - d\hat{t}^k\right) \\ &= \varepsilon_\rho^k - \delta\hat{r}^k\end{aligned} \tag{6}$$

Rewrite equation (6), the multipath error for satellite k can then be computed as:

$$\varepsilon_\rho^k = \delta b^k + \delta\hat{r}^k \tag{7}$$

Using weighted Least Square Estimation, the position error from multipath can be estimated by:

$$\boldsymbol{\delta\hat{x}}_\varepsilon = \left(\mathbf{G}^T \boldsymbol{R}_\varepsilon^{-1}\mathbf{G}\right)^{-1}\mathbf{G}^T\boldsymbol{R}_\varepsilon^{-1}\boldsymbol{\epsilon}_\rho \tag{8}$$

where $\mathbf{G}$ is the geometry matrix and $\mathbf{R}_\varepsilon$ is the error covariance matrix.

Figure **7** presents examples of the computed code bias, the corresponding code bias model, and the code bias deviations for different satellites using van test data collected in urban environments. The test begins in an open-sky area, then proceeds into the core downtown region characterized by severe multipath and signal degradation, before returning to an open-sky environment. The results show that the code bias models are properly derived and fitted using the identified open-sky data, while significant code bias deviations are observed in the core downtown area.

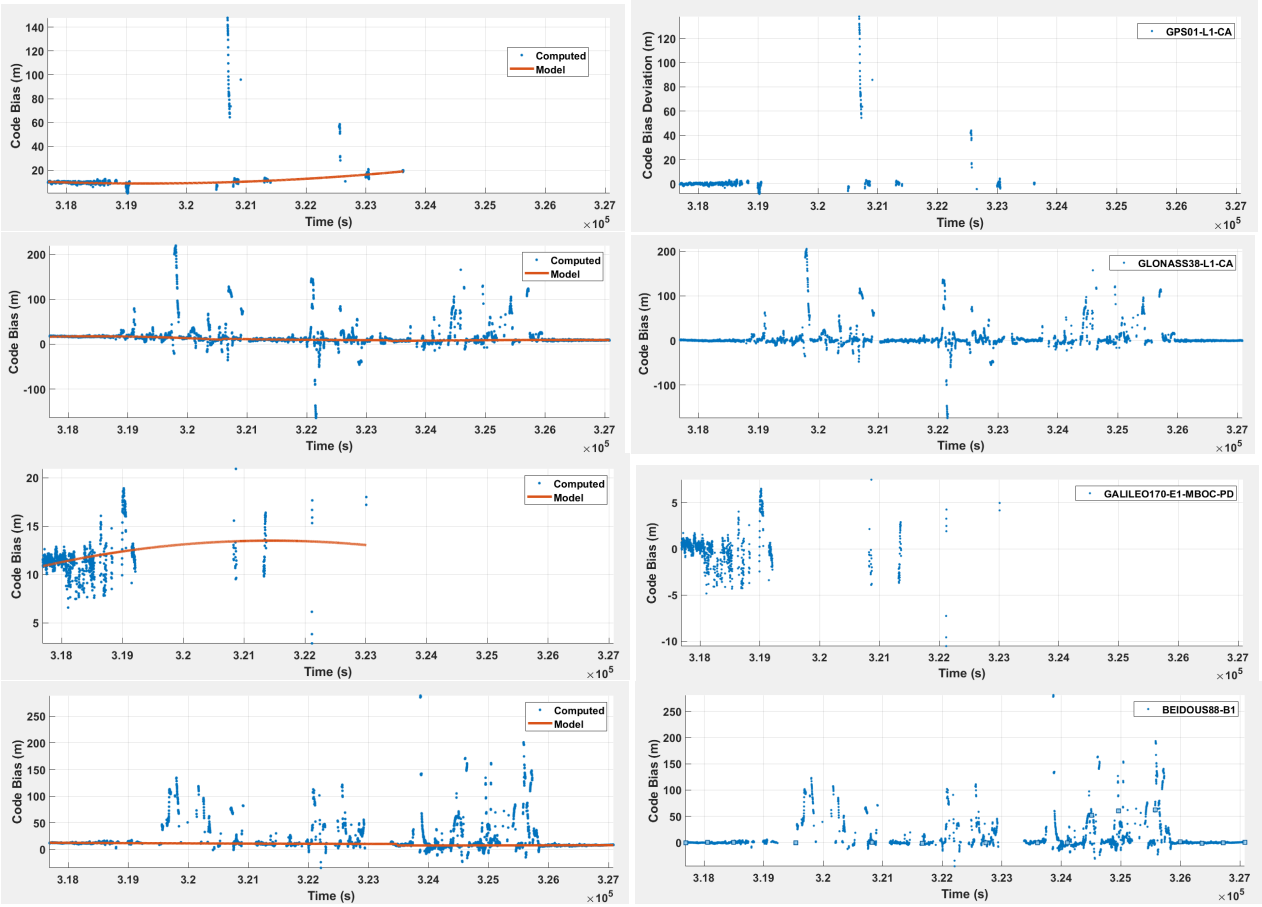

Figure 7 Code biases deviation in urban areas

Figure 8 compares the true position error with the position standard deviation output by the GNSS estimator, and the position error estimate generated by the proposed method based on code bias deviations for urban area data. The true position is provided by a highly precise GNSS/INS reference system. The results show that the position standard deviation reported by the GNSS estimator does not accurately reflect the true position error, as large position errors can occur alongside small reported standard deviations. In contrast, the position error estimates produced by the proposed method exhibit a strong correlation with the true position error and can reliably indicate positioning accuracy degradation.

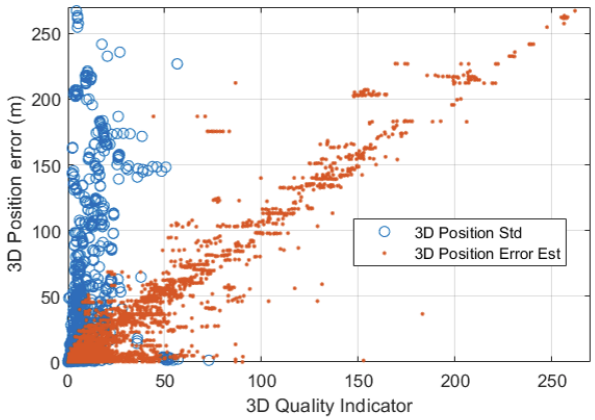

Figure 8 Position error vs position standard deviation and position error estimate in urban areas

3.4 Outlier detection and error modeling

Because the proposed method yields position error estimates that demonstrate high consistency with the ground truth, they serve as a reliable metric for identifying accuracy degradation. Consequently, these estimates can be directly integrated into the GNSS-inertial data fusion framework for both outlier detection and stochastic error modeling. Specifically, if a position error estimate exceeds a predefined threshold, the corresponding solution is classified as an outlier and excluded from the Kalman filter update to prevent filter divergence. For valid solutions that pass this threshold, the error estimates are dynamically incorporated into the GNSS-inertial measurement covariance matrix, ensuring the filter accurately reflects the current sensor uncertainty.

Figure 9 provides a comparative visualization of outlier detection performance using a 7.5 m rejection threshold. When the detection logic relies on the standard deviations reported by the GNSS estimator, significant degradation is observed, with numerous GNSS position solutions (blue) exhibiting true errors exceeding the prescribed threshold. Conversely, utilizing the proposed position error estimates ensures that the majority of solutions (orange) remain bounded within the 7.5 m limit. These findings indicate that the proposed method provides a more reliable metric for identifying GNSS outliers than conventional estimator outputs.

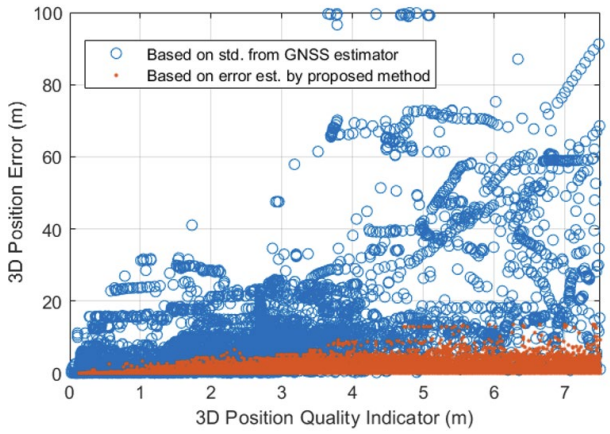

Figure 9 Validation of outlier rejection logic comparing the conventional GNSS estimator output (blue) against the proposed error estimation method (orange).

4. Performance enhancement assessment

The performance enhancement of the Trimble Applanix POSPac IN-Fusion+ PP-RTX solution via the proposed CBGOD method was validated using an extensive 65-hour dataset acquired in the urban canyons of downtown Toronto. To establish a high-fidelity ground truth, reference trajectories were generated using a navigation-grade Inertial Measurement Unit (IMU) integrated via Trimble ProPoint Single Base RTK tightly coupled processing. Data acquisition involved a heterogeneous fleet of five Trimble Applanix GNSS-inertial mobile mapping systems, including the POS LV620, LV420, LV220, AP+, and LVX models (Trimble Applanix, 2025). The test routes, shown in Figure 10, encompass a complex urban morphology of low-rise to high-rise buildings. This environment induces significant GNSS signal attenuation and multipath effects, providing a representative scenario for testing the robustness of navigation solutions. Comparative performance analysis was conducted by processing the raw data through the POSPac IN-Fusion+ PP-RTX engine, evaluating the system both with and without the integrated outlier detection framework.

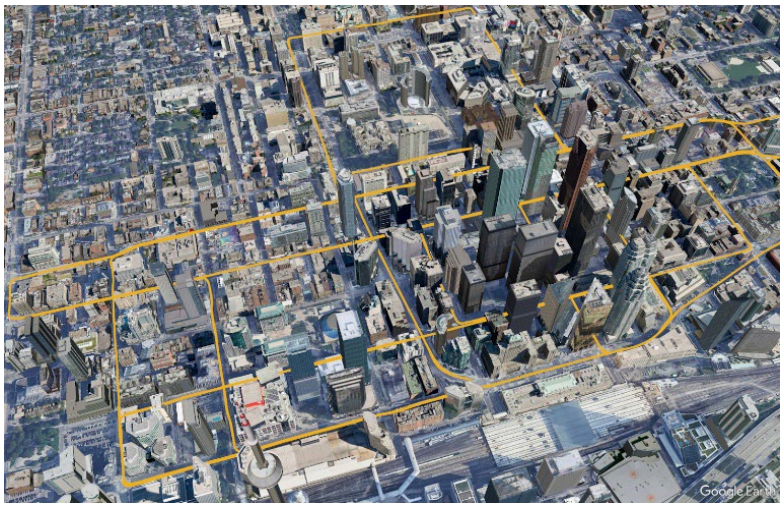

Figure 10 Downtown Toronto test trajectories

Figure 11 and Figure 12 illustrate the efficacy of the CBGOD method in enhancing the reliability of the PP-RTX solution within the downtown Toronto dataset. A comparison of the original PP-RTX position errors (blue) and the filtered errors post-outlier detection (orange) is provided in Figure 11. The results demonstrate that while standard PP-RTX trajectories are susceptible to significant excursions in dense urban environments, the CBGOD framework effectively identifies and mitigates these outliers, ensuring a more stable positioning solution. Figure 12 characterizes the relationship between the PP-RTX position errors and their corresponding reported standard deviations. Post-rejection, the remaining solutions demonstrate a high degree of consistency with their reported uncertainty, ensuring that only statistically reliable estimates are retained for the final solution.

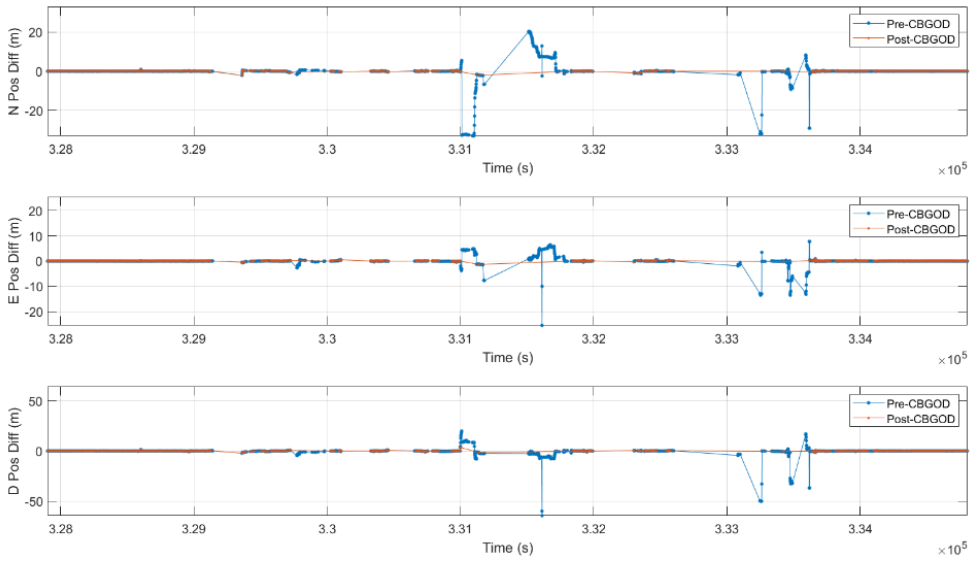

Figure 11 Comparison of PP-RTX position errors in downtown Toronto before and after the application of the CBGOD method.

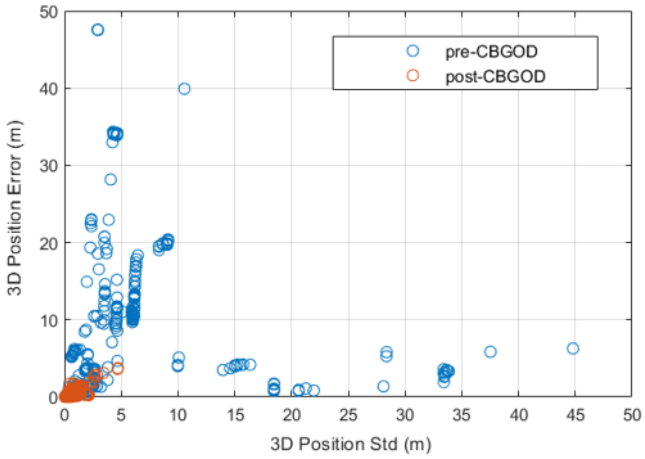

Figure 12 Relationship between PP-RTX position errors and reported standard deviations in downtown Toronto before and after the application of the CBGOD method.

Figure 13 illustrates the Cumulative Distribution Function (CDF) for the PP-RTX 3D position errors derived from the 65-hour downtown Toronto dataset, with the corresponding statistical performance summarized in Table 1. The integration of the CBGOD method yielded an 87.84% reduction in 3D positioning error at the 1σ (68.3%) confidence level, improving from a baseline of 58.06 cm to 7.06 cm. Even more significant gains were observed at the 2σ (95.4%) level, where the error decreased by 94.39%, from 1175.73 cm to 65.93 cm. These results quantify the framework's capacity to substantially mitigate large-scale urban outliers and improve overall PP-RTX solution reliability.

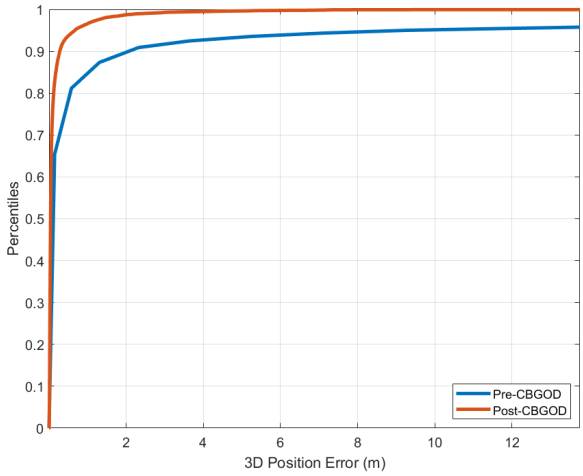

Figure 13 CDF of PP-RTX 3D position errors pre- and post-CBGOD processing for urban canyon environments

Table 1

Statistical summary of PP-RTX 3D position error performance

PP-RTX 3D position error	Pre-CBGOD	Post-CBGOD	Improvement
1σ (cm)	58.06	7.06	87.84%
2σ (cm)	1175.73	65.93	94.39%

Figure 14 illustrates the efficacy of the CBGOD method in enhancing the performance of the IN-Fusion+ PP-RTX solution within the downtown Toronto dataset. As depicted, the pre-CBGOD (baseline) PP-RTX position errors (blue) exhibit significant drift and excursions reaching over 10 meters. In contrast, the post-CBGOD solutions (orange) effectively suppress these inaccuracies, maintaining the 3D position errors within a highly constrained range of only a few meters. These results demonstrate the framework's ability to maintain high-precision positioning even in the presence of severe urban GNSS signal degradation.

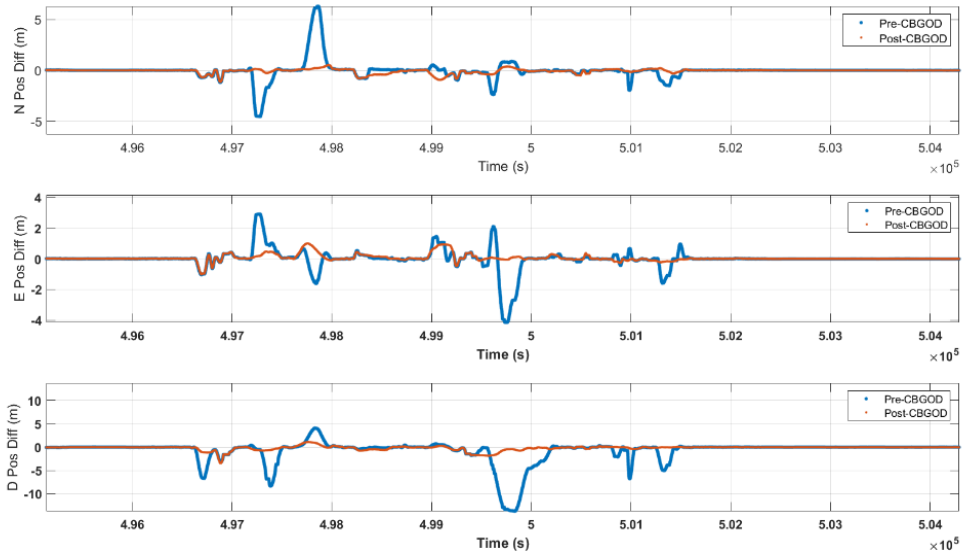

Figure 14 Comparison of IN-Fusion+ PP-RTX position errors in downtown Toronto before and after the application of the CBGOD method

Figure 15 and Table 2 characterize the 3D positioning performance of the IN-Fusion+ PP-RTX engine across 65 hours of downtown Toronto data. By deploying the CBGOD method, the baseline PP-RTX 1σ error of 115.9 cm was refined to 64.48 cm, representing a 44.37% improvement. Furthermore, 2σ error was reduced by nearly an order of magnitude, from 709.2 cm down to 298.4 cm (an 57.92% decrease). This substantial reduction in the 95.4th percentile error underscores the framework's capability to isolate and reject large-scale GNSS outliers typical of dense urban canyons. Furthermore, these results demonstrate the method's effectiveness of properly modeling PP-RTX error characteristics for robust integration within the sensor fusion engine.

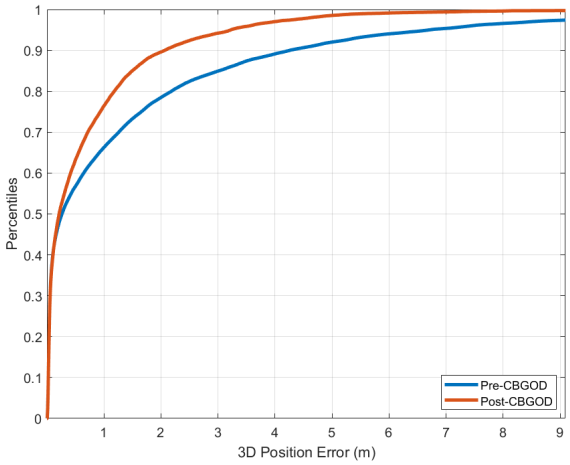

Figure 15 CDF of IN-Fusion+ PP-RTX 3D position errors pre- and post-CBGOD processing for urban canyon environments

Table 2

Statistical summary of IN-Fusion+ PP-RTX 3D position error performance

IN-Fusion+ PP-RTX 3D position error	Pre-CBGOD	Post-CBGOD	Improvement
1σ (cm)	115.9	64.48	44.37%
2σ (cm)	709.2	298.4	57.92%

5. Conclusion

This paper introduced a novel GNSS outlier detection method to improve the robustness of the Trimble PP-RTX solution and enhance IN-Fusion+ PP-RTX inertial navigation performance in urban canyon environments. The proposed approach identifies multiple concurrent measurement outliers using only raw GNSS observations, provides effective detection of large-error PP-RTX solutions and improves PP-RTX error modeling within the GNSS-inertial fusion filter. The method was validated using 65 hours of real-world urban canyon data and resulted in two patent applications (Wang, 2025a, 2025b). Experimental results demonstrate consistent and substantial accuracy improvements for both standalone PP-RTX and IN-Fusion+ PP-RTX inertial navigation solutions. The results confirm the effectiveness and robustness of the proposed method and its suitability for high-precision GNSS-inertial post-processing in urban and other signal-challenged environments.

References

Anyaegbu E., & Hansen P. (2022). GNSS Performance Evaluation for Deep Urban Environments using GNSS Foresight. *Proceedings of the 35th International Technical Meeting of the Satellite Division of The Institute of Navigation (ION GNSS+ 2022), Denver, CO*

Brown, R. G. (1996). Receiver autonomous integrity monitoring. *Global Positioning System: Theory and Applications, Volume II, B. W. Parkinson and J. J. Spilker Jr, Eds. Washington DC: AIAA*, ch. 5, 143–165.

Castaldo, G., Angrisano, A., Gaglione, S., & Troisi, S. (2014). P-RANSAC: An Integrity Monitoring Approach for GNSS Signal Degraded Scenario. *International Journal of Navigation and Observation*, Vol. 2014, Article ID 173818.

Gangi, A. F. & Shapiro J. N. (1997). A propagating algorithm for determining nth-order polynomial, least-squares fits, *Geophysics* Vol. 42, No. 6, 1265–1276

Hutton, J., Gopaul, N., Zhang, X., Wang, J., Menon, V., Rieck, D., Kipka, A., & Pastor, F. (2016). Centimeter-level robust GNSS-aided inertial post-processing for mobile mapping without local reference stations, *Int. Arch. Photogramm. Remote Sens. Spatial Inf. Sci.,* XLI-B3, 819–826, https://doi.org/10.5194/isprs-archives-XLI-B3-819-2016.

Kuusniemi, H., Wieser, A., Lachapelle, G., & Takala, J. (2007). User-level reliability monitoring in urban personal satellite-navigation. *IEEE Transactions on Aerospace and Electronic Systems*, Vol. 43, Issue 4, 1305-1318

Leandro, R., Landau, H., Nitschke, M., Glocker, M., Seeger, S., Chen, X., Deking, A., BenTahar, M., Zhang, F., Ferguson, K., Stolz, R., Talbot, N., Lu, G., Allison, T., Brandl, M., Gomez, V., Cao, W., & Kipka, A. (2011) RTX Positioning: The Next Generation of cm-accurate Real-time GNSS Positioning, *Proceedings of the 24th International Technical Meeting of the Satellite Division of The Institute of Navigation (ION GNSS 2011), Portland, OR*, 1460-1475.

Li, B., Dan, Z., Fang, K., Guo, K., Wang, Z., & Zhu, Y. (2022). A LiDAR Aided Real-time GNSS Fault Detection Algorithm in Urban Environments. *Proceedings of the 2022 International Technical Meeting of The Institute of Navigation, Long Beach, CA*

Scherzinger, B & Hutton, J. (2020). Applanix IN-Fusion+™: the Ultimate Solution for Enhanced Spatial Intelligence *Trimble Applanix*

Trimble Applanix. (2025). Mobile Mapping Products: POS LV and AP+ Series Specifications. Retrieved from https://applanix.trimble.com/en

Wang, J-H., & Gao Y. (2007). High Sensitivity GPS Data Classification based on Signal-Degraded Conditions. *IEEE Transactions on Vehicular Technology*, Vol. 56, Issue 2, 566-574.

Wang, J-H. (2025a) GNSS Position Outlier Detection Using Code Bias Deviation, *U.S. Patent Application* No. 19/094,168, filed March 28, 2025.

Wang, J-H. (2025b) GNSS Observable Outlier Detection And Removal, *U.S. Patent Application* No. 19/094,154, filed March 28, 2025.